J Mater Sci: Mater Electron (2016) 27:8550–8558
DOI 10.1007/s10854-016-4872-z

CrossMark

Influences of rapid thermal annealing on the characteristics of $Al_2O_3\backslash La_2O_3\backslash Si$ and $La_2O_3\backslash Al_2O_3\backslash Si$ films deposited by atomic layer deposition

Chenxi Fei[1] · Hongxia Liu[1] · Xing Wang[1] · Dongdong Zhao[1] · Shulong Wang[1]

Received: 27 February 2016 / Accepted: 19 April 2016 / Published online: 29 April 2016
© Springer Science+Business Media New York 2016

Abstract A comparative study of different sequences of two metal precursors [trimethylaluminum (TMA) and Tris(isopropylcyclopentadienyl) lanthanum (La(^{i}PrCp)$_3$)] for atomic layer deposition (ALD) lanthanum aluminum oxide ($La_2O_3/Al_2O_3/Si$) films is carried out. The percentage compositions of C and N impurity of $La_2O_3/Al_2O_3/Si$ and $Al_2O_3/La_2O_3/Si$ films were investigated using in situ X-ray photoelectron spectroscopy (XPS). The preliminary testing results indicate that the impurity level of films grown with different sequences before and after annealing can be well controlled. The effects of different deposition sequences on the electrical characteristics and physical properties of $La_2O_3/Al_2O_3/Si$ and $Al_2O_3/La_2O_3/Si$ films before and after annealing are studied by atomic force microscopy (AFM) and C–V curves. Analysis indicates the rapid thermal annealing (RTA) has significant effects on the surface roughness, equivalent oxide thickness (EOT), dielectric constant, electrical properties, and stability of different sequences of films. Additional the change of chemical bond types of RTA effects on the properties of $La_2O_3/Al_2O_3/Si$ and $Al_2O_3/La_2O_3/Si$ films are also investigated by XPS.

1 Introduction

Numerous scientific and technological challenges have to be surmounted to continue Moore's law, which predicts that the device density wills double every 18–24 months. The miniaturization of complementary metal–oxide–semiconductor (COMS) technology has pushed the conventional silicon dioxide (SiO_2) gate dielectric close to its physical limit. As the thickness of SiO_2 gate dielectric decrease, it becomes more difficult to grow high quality oxides because boron penetration, excessive tunneling, and reliability of ultra-thin SiO_2 will seriously degrade the device performance. Therefore, high-*k* materials have attracted considerable attentions lately because they can be physically thicker, reducing leakage currents while maintaining electric properties, thereby providing opportunity for additional scaling [1–4]. Consequently, there has recently been a major research effort aimed at replacing the existing SiO_2 gate dielectric with alternative high-*k* dielectric oxides such as Al_2O_3, HfO_2, Nd_2O_3, ZrO_2 [5–13] and their pseudobinary [14–19]. However, many of these materials are not thermally stable on the silicon substrate: Either at deposition or during subsequent annealing treatments, the electrical properties of high-*k* films can suffer severe degradation due to interface reactions, or crystallization of as-deposited amorphous films. Besides, the formation of an interfacial layer (IL) between the high-*k* film and the substrate due to oxidation of the substrate by excess oxygen in the bulk high-*k* film or during its initial stages of deposition causes a substantial reduction of the dielectric constant.

Among the high-*k* dielectrics, La_2O_3 is known to be superior in terms of both thermodynamic stability and high dielectric constant (~ 27). However, La_2O_3 can easily form both La-silicate and La-hydroxide because of the catalytic and hygroscopic behavior of La_2O_3 film. It will cause the decrease of the dielectric constant and performance degradation of the films. Al_2O_3 has many favorable properties like large band gap, kinetic stability, thermodynamic stability on Si up to high temperatures, good interface with silicon, low bulk defect density and is amorphous under the conditions of

✉ Hongxia Liu
hxliu@mail.xidian.edu.cn

[1] Key Laboratory for Wide-Band Gap Semiconductor Materials and Devices of Education, School of Microelectronics, Xidian University, Xi'an 710071, China

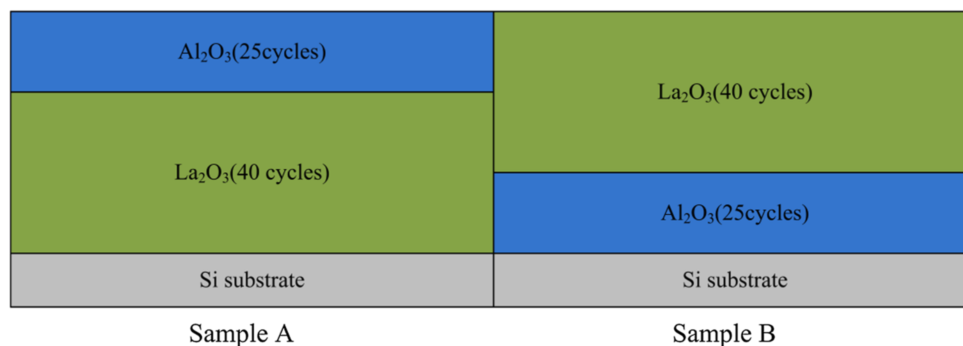

Fig. 1 Schematic drawings for two kinds of Al_2O_3/La_2O_3 laminate profiles (Al_2O_3/La_2O_3/Si and La_2O_3/Al_2O_3/Si)

Table 1 The percentage compositions of C and N impurities for samples

Sample	C (at%)	N (at%)
A	3.95	1.93
B	3.47	1.65
C	2.64	1.32
D	2.81	1.19

interest. In particular the high chemical stability and high thermal conductivity make it suitable for application in MOS structures even in drastic conditions. Al_2O_3 also has others applications such as passivation layers and dielectric films in chemical sensors. All these applications require Al_2O_3 films with good homogeneity, low surface roughness and good control of thickness for films. Al_2O_3 is one of the best high-*k* materials which satisfy almost all the guidelines for an ideal gate oxide. On the other hand, $LaAlO_3$, which is a compound of La_2O_3 and Al_2O_3, has high immunity against moisture in the environment. Its thermal stability on Si is similar to that of La_2O_3 on Si, and its dielectric constant (25–27) is nearly the same as that of La_2O_3 [20, 21]. However, the different sequences of La_2O_3 and Al_2O_3 layers on the electrical and physical characteristics of silicon-based films have rarely been discussed. Therefore, in this paper, different sequences of La_2O_3/Al_2O_3/Si films are deposited by atomic layer deposition (ALD). The effects of the different deposition sequences on the electrical characteristics, physical properties, surface behaviour and chemical bonding structure of La_2O_3/Al_2O_3/Si and Al_2O_3/La_2O_3/Si films are investigated before and after annealing.

2 Experimental details

La_2O_3/Al_2O_3/Si and Al_2O_3/La_2O_3/Si films were grown in a Picosun R-200 ALD reactor (Espoo, Finland) on p-type Si (8–12 Ω cm) B-doped (100) wafers. The H-terminated Si (100) was obtained after cleaning ($HCl:H_2O_2:H_2O$ = 1:1:5, 10 min at 85 °C) and a 30 s dip in a diluted HF solution ($HF:H_2O$ = 1:50, at room temperature), both followed by a 30 s rinse in deionized water. For ALD film deposition, trimethylaluminum (TMA) and $La(^iPrCp)_3$ were used as precursors, H_2O was used as oxidant, ultra-high purity nitrogen (N_2, 99.999 %) was employed as carrier and purge gas. The vapor pressure of container was kept in 10–15 hPa. La_2O_3 films were deposited at a growth temperature of 290 °C alternating pulses of $La(^iPrCp)_3$ and H_2O; the layers thickness was tuned varying the number of ALD cycles. ALD cycle structure was composed of 0.5s $La(^iPrCp)_3$ pulse/6s purge with N_2/0.5s H_2O pulse/8s purge with N_2. La source was kept at 180 °C; Al_2O_3 films were deposited at a growth temperature of 290 °C alternating pulses of TMA and H_2O; ALD cycle structure was composed of 0.1s TMA pulse/3s purge with N_2/0.1s H_2O pulse/4s purge with N_2. Al source was kept at room temperature.

40 cycles La_2O_3 and 25 cycles Al_2O_3 layers (Sample A), 25 cycles Al_2O_3 and 40 cycles La_2O_3 layers (Sample B) shown in Fig. 1 were subsequently deposited at 290 °C, respectively, as high-*k* dielectric oxides. Also, after the deposition of the sample A and sample B, high temperature annealing processing using Rapid Thermal Processing (RTP) was performed at 500 °C for 1 min in N_2 atmosphere. Sample A and sample B after annealing were marked as sample C and sample D, respectively. Film thicknesses were measured by J. A. Woollam M2000D spectroscopic ellipsometry. The capacitance–voltage (C–V) measurements were carried out using a Keithley 590 C–V analyzer (Keithley Instruments Inc., Cleveland, OH, USA) at 100 kHz, the diameter of mercury probe is 859 microns. The bonding structures of the films were examined by X-ray photoelectron spectroscopy (XPS). The atomic force microscopy (AFM) of the films were measured by Seiko SPI3800-SPA-400 scanning probe microscope (Seiko Instruments Inc., Chiba, Japan). The physical thickness of the gate dielectric films was measured by cross-section high-resolution transmission electron microscopy (HRTEM).

3 Results and discussion

The XPS quantitative analysis is performed to determine the chemical composition of the film, and the results are shown in Table 1. The percentage compositions of C

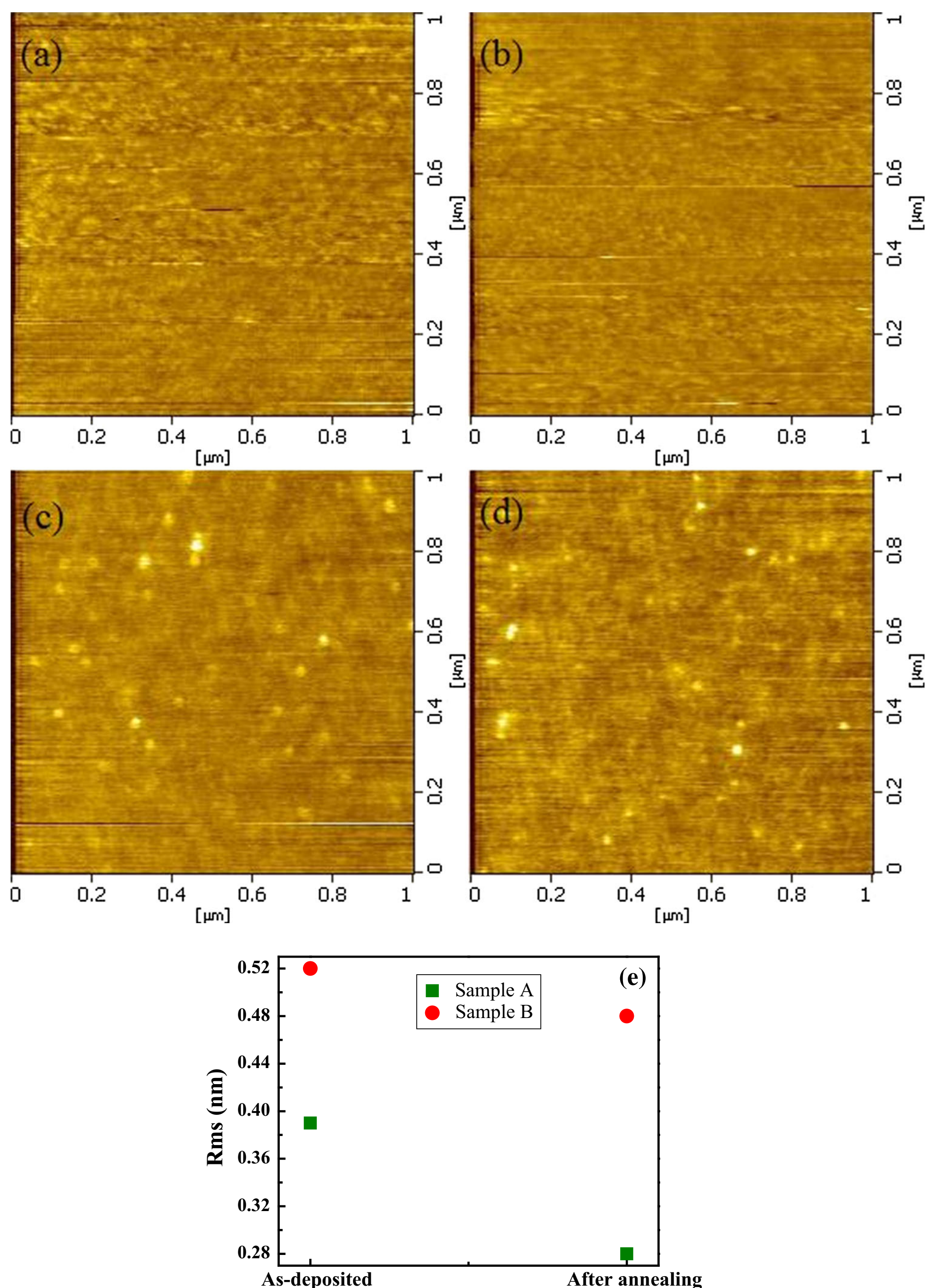

Fig. 2 AFM images of samples. **a** Sample A. **b** Sample B. **c** Sample C. **d** Sample D. **e** Surface roughness values of all films before and after annealing

impurity for Sample A and Sample C are 3.95 and 2.64 %; percentage compositions of C impurity for Sample B and Sample D are 3.47 and 2.81 %, respectively. The residual C impurity mainly comes from the residues of metal precursors or C containing groups attached to the metal atoms for the as-deposited samples. The content of C impurity for sample A and Sample B decreases significantly after annealing. This result indicates that the film after annealing is more likely to achieve the saturate reaction compared with the as-deposited film, and has an advantage in controlling the C impurity level. This attributed to the unstable bonds can decompose in the annealing process. Furthermore, the percentage compositions of N impurity for Sample A and Sample C are 1.93 and 1.32 %; percentage compositions of N impurity for Sample B and Sample D are 1.65 and 1.19 %, respectively. The residual N impurity mainly comes from the formation of La–N and Si–N bonding. The La–N bonding is detected in the film resulting from the incomplete reaction of the amidinate ligands of the La precursor during the oxidant pulse, which

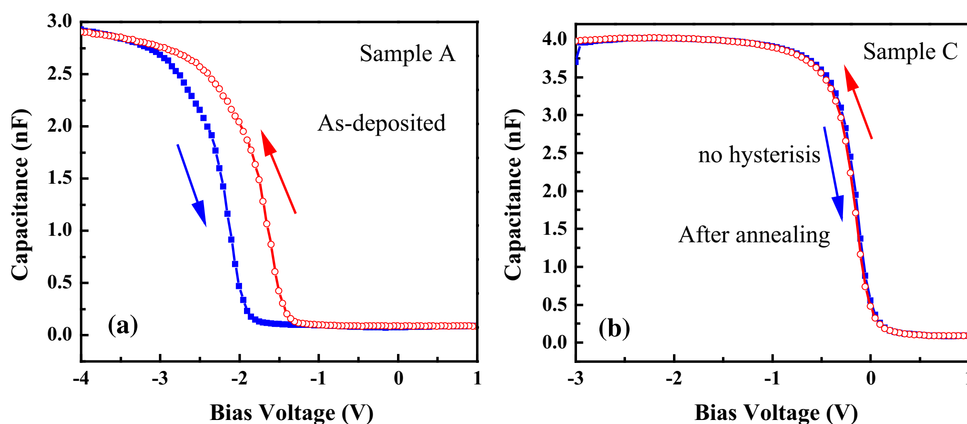

Fig. 3 C–V characteristics for different samples. **a** Sample A. **b** Sample C

is defined as residual N-related impurities [8]. N in the La precursor also formed Si–N bonding at the interface between the film and Si substrate during ALD. In the annealing process, these unstable bonds can decompose and the content of N impurity decreases [22]. In summary, the content of C and N impurities for $La_2O_3/Al_2O_3/Si$ and $Al_2O_3/La_2O_3/Si$ films decreased after annealing. These phenomena mainly attributed to the unstable bonds which influence the property of films can decompose during the rapid thermal annealing (RTA) process. Films are more likely to achieve the saturate reaction and possess good characteristics after annealing.

AFM analyses on the morphology of the $Al_2O_3/La_2O_3/Si$ and $La_2O_3/Al_2O_3/Si$ thin films definitely showed that ALD could be utilized to deposit very smooth and uniform films. AFM studies on the films morphology are shown in Fig. 2, with scanned areas of 1 μm × 1 μm for each sample. For the four samples, the surface roughness of samples were measured 0.39, 0.52, 0.28 and 0.48 nm are shown in Fig. 2e. In Fig. 2a, the $Al_2O_3/La_2O_3/Si$ surface is rougher than that in Fig. 2c; in Fig. 2b, the $La_2O_3/Al_2O_3/Si$ surface is rougher than that in Fig. 2d. The RMS decreased after annealing for sample A and B, this indicates that the RTA process enhances surface smoothness of films. On the other hand, the RMS of $Al_2O_3/La_2O_3/Si$ film is smoother than of $La_2O_3/Al_2O_3/Si$ film before and after annealing. For sample A, Al_2O_3 deposited on the top of film. To a certain extent, the reaction of La_2O_3 and moistures are prevented. For sample B, La_2O_3 deposited on the top of film. The $La(OH)_3$ in formed during preserved in air and the RTA process [23, 24]. The formation of La-hydroxide increases the RMS of films. In general, all films are deposited on Si substrate with uniform surface morphology.

Figure 3 shows C–V characteristics of the Sample A before and after annealing. Al 2*p*, O 1*s* and La $3d_{5\backslash 2}$ XPS spectra of Sample A before and after annealing are shown in Fig. 4. The binding energies of core levels are calibrated by setting the adventitious carbon 1*s* peak at 284.6 eV. The Al 2*p*, O 1*s* and La $3d_{5\backslash 2}$ spectrums of the films with Ar^+ sputtering for 20 s. The Al 2*p* spectrum was fitted with two peaks after the application of a Smart background shown in Fig. 4a. Blue and green curves stand for the La–O–Al and Al–O–Al peaks respectively. The existence of La–O–Al indicates the formation of $LaAlO_x$ at $Al_2O_3/La_2O_3/Si$ contact layer. The existence of Al–O–Al attributed to the formation of Al_2O_3 on the top of films. The areas of La–O–Al peak decreased and areas of Al–O–Al peak increased after annealing. This mainly due to a small amount of La–O–Al decomposed and formed Al–O bonds during RTA process [6, 25]. In Fig. 3a, blue and red lines represented gate bias swept from negative to positive and followed by an opposite direction, respectively. A hysteresis loop appeared in Sample A, this attributed to the formation of trapped charge in the films, which caused by formation of La-silicate. Furthermore, the O 1*s* spectrum was fitted with three peaks after the application of a Smart background shown in Fig. 4b. Blue, green and pink curves stand for the La–O–La, La–OH and La–O–Si peaks respectively. The existence of La–OH and La–O–Si peaks attributed to the formation of $La(OH)_3$ and La-silicate. La–OH and La–O–Si bonding peaks mainly caused by the moisture adsorption of La_2O_3 and a diffusion of La atoms into Si substrate respectively [6, 26]. La $3d_{5\backslash 2}$ spectrum was fitted with three peaks after the application of a Smart background shown in Fig. 4c. Pink, red and green curves stand for the La–O–Al, La–O–La and La–O–Si peaks respectively. The hysteresis loop disappeared after annealing at 500 °C shown in Fig. 3b, this indicates the lower interface trapped charge density of interface of the film after annealing [23]. On the other hand, the areas of La–O–Si peaks decreased after annealing shown in Fig. 4b, c. This proved the property of interfacial layer have been improved after annealing which coincides with the analyse of C–V curves. Moreover, the accumulation capacitance increased after annealing, this attributed to a decrease of the concentration of interfacial fixed charge and defects [5]. We can also see in Fig. 3 that

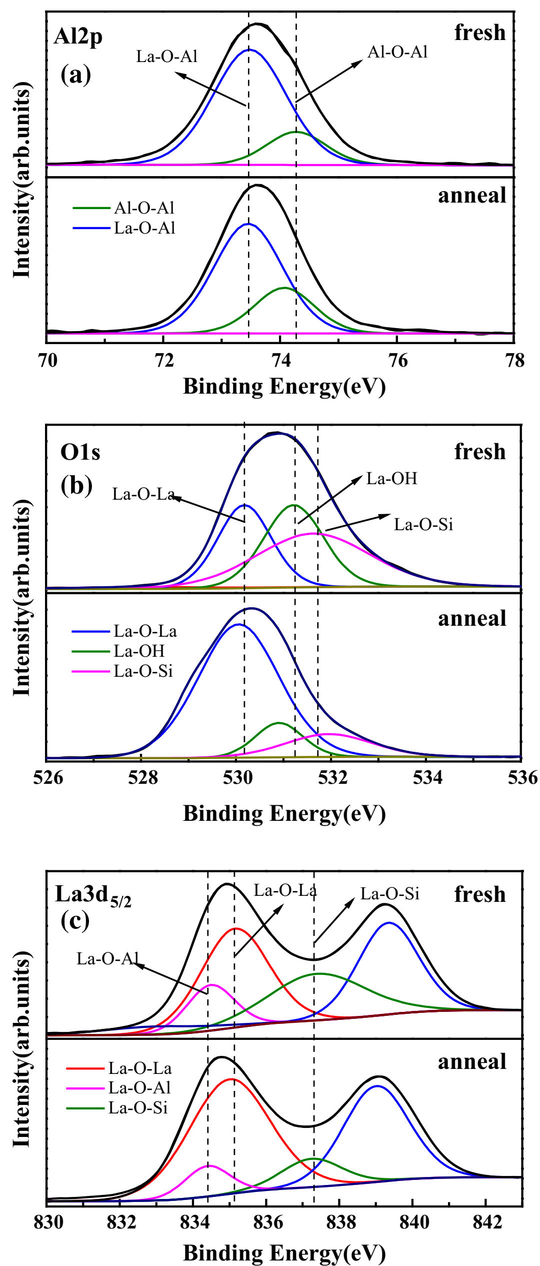

Fig. 4 XPS spectra of the $Al_2O_3/La_2O_3/Si$ nanolaminates before and after annealing. **a** Al 2*p*. **b** O 1*s*. **c** La $3d_{5/2}$

the flat band voltage is shifted in a negative direction for as-deposited film. This also caused by formation of La-silicate and indicated that positive fixed charges in film. The flat band voltages shifted toward negative voltages is strongly reduced after annealing at 500 °C. This indicates that the formation of positive charges was reduced in film and makes the films obtained better quality.

Figure 5 shows C–V characteristics of the Sample B before and after annealing. Al 2*p*, O 1*s* and La $3d_{5\backslash 2}$ XPS spectra of Sample B before and after annealing are shown in Fig. 6. In Fig. 5, blue and red lines represented gate bias swept from negative to positive and followed by an opposite direction, respectively. The hysteresis loops are insignificant of Sample B before annealing shown in Fig. 5a. However, in Fig. 5b, the hysteresis voltage was 50 mV for Sample B after annealing. Dues to Al_2O_3 have favorable properties like kinetic stability, thermodynamic stability on Si up to high temperatures, good interface with silicon. This indicates that less trapped charges are formed in films before annealing. The trapped charges increased after annealing attributed to the decomposition and recombination of chemical bonds in interfacial layer. The interfacial layer may consist of massive $AlSiO_x$ and a few $LaSiO_x$. Unlike Sample A, the Al 2*p* spectrum was fitted with three peaks after the application of a Smart background before and after annealing shown in Fig. 6a. The existence of Al–O–Si indicates the formation of Al–silicate at Al_2O_3/Si interfacial layer. The areas of Al–O–Al peak decreased and areas of Al–O–Si peak increased after annealing. This indicates that some Al atoms separated from Al–O–Al bonds and reacted with SiO_2 to form Al–silicate during the RTA process. This caused a increasing of IL and equivalent oxide thickness (EOT). O 1*s* spectrum was fitted with three peaks after the application of a Smart background shown in Fig. 6b. Green, blue and red curves stand for the La–O–La, La–OH and Al–O–Si peaks respectively. The area of Al–O–Si peak increased after annealing, this result is in accord with the analyse of Al 2*p* spectrum. On the other hand, the accumulation capacitance decreased after annealing. This attributed to the long time preserved in air after deposition for film and the hygroscopicity of La_2O_3 film, which causes the formation of $La(OH)_3$. This will cause the decrease of dielectric constant of film. Moreover, the areas of La–O–La peak decreased and areas of La–OH peak increased after annealing shown in Fig. 6b, c. Due to prolonged exposure to air and the strong hygroscopicity of La_2O_3 film, a portion of La atoms separated from La–O–La bonds and reacted with moisture in the air to form $La(OH)_3$ [25, 27]. The XPS result is in accord with the characteristics of C–V curves. Furthermore, the flat band voltage is shifted in a positive direction after annealing at 500 °C shown in Fig. 6. The shift in the flat band voltage caused by oxide defect states is induced by the diffusion of SiO_2 and Al_2O_3 [24]. The formation of SiO_2 caused by the diffusion of Si atoms and decreased dielectric constant of film.

Figures 3a and 5a show C–V characteristics of the Sample A and Sample B before annealing. Sample A, the La_2O_3 and Al_2O_3 layers were orderly deposited on the Si substrate, shows an obvious hysteresis loop. By comparison with Sample A, the hysteresis loop of Sample B which deposited the Al_2O_3 and La_2O_3 layers on the Si substrate orderly is negligible. This indicates that more trapped charges were formed in Sample A than in Sample B during ALD process. This phenomenon caused by the different

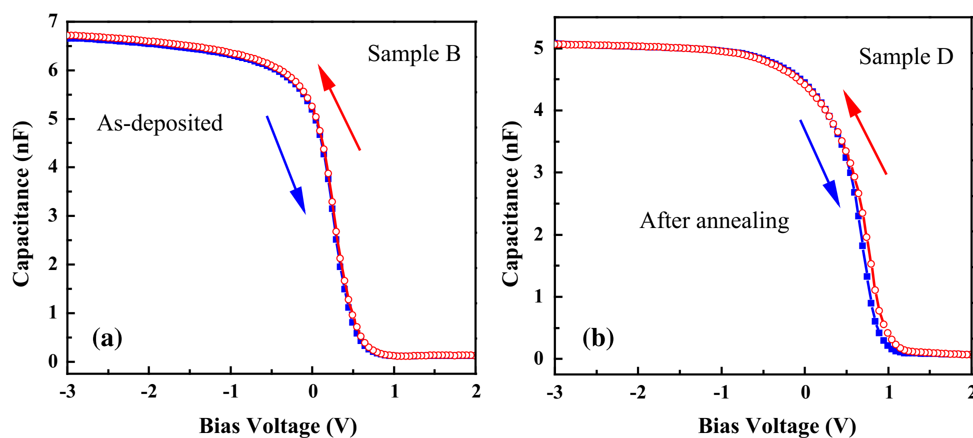

Fig. 5 C–V characteristics for different samples. **a** Sample B. **b** Sample D

interfacial characteristics of La_2O_3 and Al_2O_3 layers with Si substrate. For Sample A, the interfacial layer attributed to the formation of $LaSiO_x$, $LaAlSiO_x$ and $AlSiO_x$ which dues to the interdiffusion of La, Al, O atoms belong to La_2O_3 and Al_2O_3 films and Si atoms which came from Si substrate. However, for Sample B, the interface layer attributed to the formation of $AlSiO_x$. The Al–O–Si bond shown in Fig. 6b indicates the formation of $AlSiO_x$. Because of the favorable property of good interface with silicon of Al_2O_3 film, which can reduce the extent of diffusion for La atoms and Si atoms and the formation of La-silicate. Moreover, the variety of hysteresis loops after annealing for Sample A and Sample B shown in Figs. 3b and 5b indicates the unstable chemical bonds in the interface layer decomposed and recombined during RTA process. Generally, the two kinds of films both contained La_2O_3 layer which can react to moisture easily and form the La-hydroxide which possess low dielectric constant. In Figs. 4b, c and 6b, c, the observation of La–OH bonds indicates the formation of La-hydroxide. Moreover, the accumulation capacitances of $Al_2O_3/La_2O_3/Si$ films are smaller than the accumulation capacitances of $La_2O_3/Al_2O_3/Si$ films before and after annealing, respectively. This attributed a low concentration of interfacial fixed charge and defects in $La_2O_3/Al_2O_3/Si$ films. The phenomenon indicates the property of interfacial layer is the main reason that influences the characteristic of whole film.

Table 2 shows the numerical values of thickness, EOT and dielectric constant of samples. The extracted dielectric constant and EOT before and after annealing of sample A and sample B are shown in Fig. 7 respectively. EOT was calculated using the NCSU CVC program [28]. Films thickness of Sample A, B, C and D were measured to be 6.37, 6.08, 7.22 and 6.46 nm, respectively. In order to prove the physical thickness of films, a TEM study was carried out. Cross-sectional HRTEM images of Sample A and C are shown in Fig. 8. For Sample A and C, as indicated in the images shown in Fig. 8a, b, four different regions consisting of Al_2O_3, La_2O_3, interfacial layer and Si substrate are observed. The thicknesses of the interfacial layer of Sample A and C are 0.3 and 0.5 nm; the thicknesses of the high-k materials of Sample A and C are 6.0 and 6.7 nm, respectively. The increasing of interfacial layer of $Al_2O_3/La_2O_3/Si$ film after annealing attributed to the interdiffusion of La_2O_3, Al_2O_3 layer and Si substrate. The increasing of interfacial layer of $La_2O_3/Al_2O_3/Si$ film after annealing mainly caused by the interdiffusion of Al atoms come from Al_2O_3 layer and Si atoms come from substrate. The increasing of physical thicknesses of Sample A and B after annealing attributed to the increasing of interfacial layers and formation of lanthanum hydroxide. The analysis of HRTEM images in accord with the test result of spectroscopic ellipsometer.

The growth rate of physical thickness for Sample A is larger than the growth rate of physical thickness for Sample B after annealing. This phenomenon mainly attributed to interfacial layer that formed by different kinds of metallic silicides. The interfacial layer contained $LaSiO_x$, $LaAlSiO_x$ and $AlSiO_x$ for Sample A while the interfacial layer only contained a large number of $AlSiO_x$ and a few $LaSiO_x$ for Sample B. The situation of decomposed and recombined of chemical bonds in the interface layer of Sample B is simpler than that of Sample A. On the other hand, the physical thickness for Sample A is larger than the growth rate of physical thickness for Sample B before after annealing. This indicates the property of interfacial layer serious influence the thickness of the two kinds of films, especially for $Al_2O_3/La_2O_3/Si$ films. Moreover, the increasing of thickness for films after annealing indicates that the interfacial layer was formed during the RTA process. For Sample A, $Al_2O_3/La_2O_3/Si$ film, EOT decreased and dielectric constant increased after annealing. In Fig. 7a,

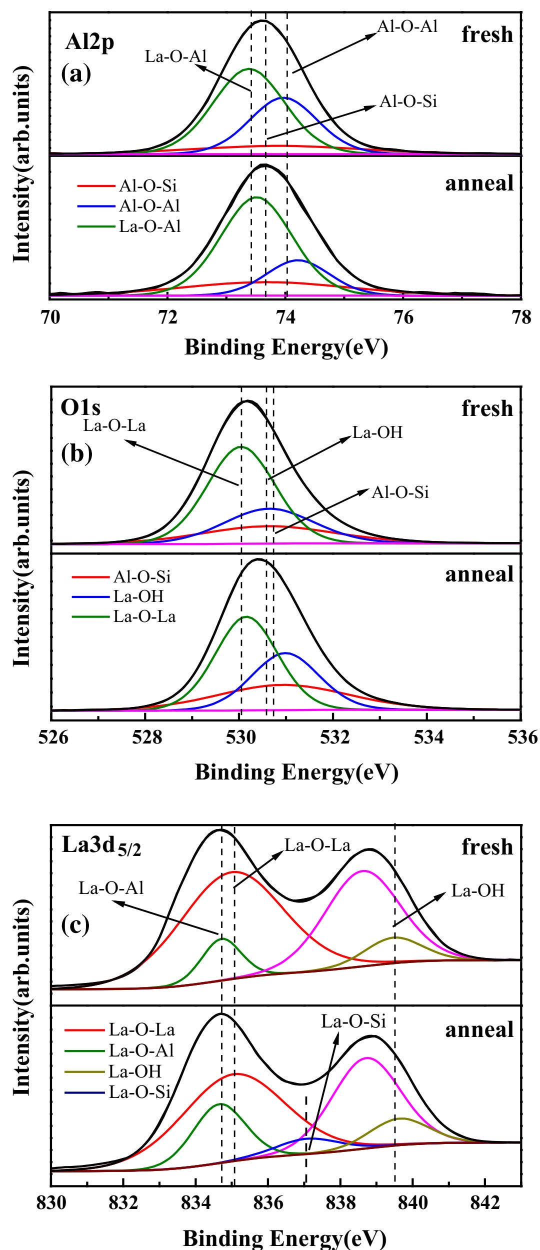

Fig. 6 XPS spectra of the $La_2O_3/Al_2O_3/Si$ nanolaminates before and after annealing. **a** Al 2*p*. **b** O 1*s*. **c** La $3d_{5/2}$

Table 2 Numerical values of thickness, EOT and dielectric constant of samples

Sample	Thickness (nm)	EOT (nm)	Dielectric constant
A	6.37	5.17	4.80
B	6.08	2.24	10.59
C	7.22	3.75	7.51
D	6.46	2.94	8.56

EOT is 5.17 nm for Sample A; EOT decreased to 3.75 nm after annealing. The reduction of EOT mainly attributed to the increasing of accumulation capacitance. The La, Si and O atoms recombined in interface layer during the RTA process, this caused a decrease of the concentration of interfacial fixed charge and defects. This indicates that the RTA process can improve the quality of interfacial layer of $Al_2O_3/La_2O_3/Si$ film. On the other hand, dielectric constant is 4.8 for Sample A; dielectric constant increased to 7.51 after annealing. The increasing of dielectric constant attributed to increasing of accumulation capacitance and reduction of impurity. In Fig. 4b, c, the increasing of area of La–O–La bonds and reduction of area of La–OH and La–O–Si bonds indicate the enhance of dielectric constant and decrease of EOT of $Al_2O_3/La_2O_3/Si$ film after annealing, which is fit to the result obtained by variations of EOT and dielectric constant [29, 30]. On the contrary, for Sample B, $La_2O_3/Al_2O_3/Si$ film, EOT increased and dielectric constant decreased after annealing. In Fig. 7b, EOT is 2.24 nm for Sample B; EOT decreased to 2.94 nm after annealing. The increasing of EOT mainly attributed to the reduction of accumulation capacitance, which caused by a formation of SiO_2 layer and Al–silicate in interface layer during the RTA process. On the other hand, dielectric constant is 10.59 for Sample B; dielectric constant decreased to 8.56 after annealing. There are two reasons for the reduction of dielectric constant: Firstly, the formation of Al–silicate in interface layer; moreover, the formation of La-hydroxide. As is known to all, La_2O_3 film can react to moisture easily and form $La(OH)_3$ [31]. Contacting with moistures is unavoidable before and during the RTA process. The dielectric constant of $La(OH)_3$ is very low, therefore, the formation of $La(OH)_3$ decreases whole dielectric constant of film. In Figs. 6b, c, the increasing of area of La–OH bonds and reduction of area of La–O–La bonds indicate the enhance of EOT and decrease of dielectric constant of $La_2O_3/Al_2O_3/Si$ film after annealing, which is in accord with the result obtained by variations of EOT and dielectric constant. Furthermore, the La–O–Si peak with blue curve was observed after annealing in La $3d_{5\backslash 2}$ XPS spectra shown in Fig. 6c. This implies that a number of La atoms diffused through Al_2O_3 film into SiO_2/Si interfacial layer to form La silicate during the RTA process. The formation of La silicate also increased value of EOT.

It is observed that the characteristics of EOT and dielectric constant of $La_2O_3/Al_2O_3/Si$ films are superior to the characteristics that of $Al_2O_3/La_2O_3/Si$ films before and after annealing. In summary, the improvement of property of interface layer is obvious for $Al_2O_3/La_2O_3/Si$ film after

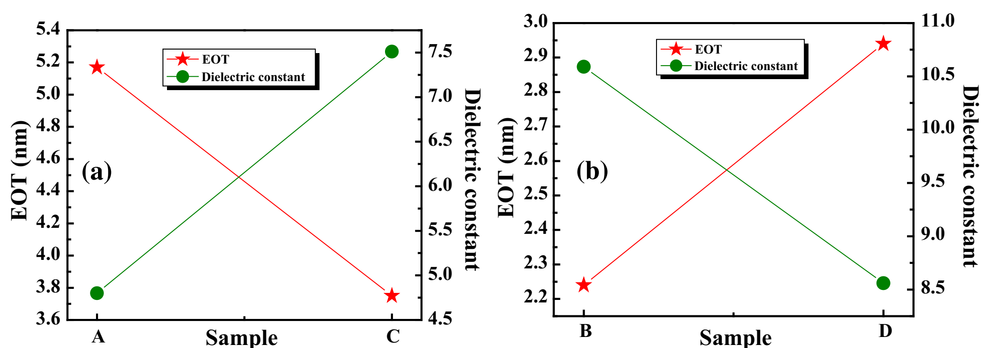

Fig. 7 Values of EOT and dielectric constant of the samples. **a** Sample A and sample C. **b** Sample B and sample D

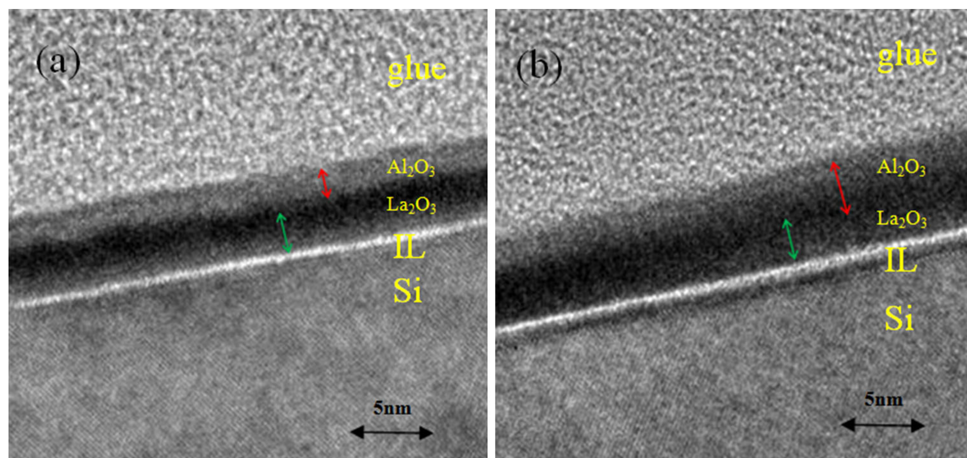

Fig. 8 HRTEM images of samples. **a** Sample A. **b** Sample C

annealing. The EOT decreased and the dielectric constant increased during RTA process. However, the dielectric constant (7.51) of $Al_2O_3/La_2O_3/Si$ film after annealing is smaller than the theoretical values of dielectric constant of La_2O_3 ($\sim$27) and Al_2O_3 ($\sim$9) films. This mainly attributed to the formation of complicated interfacial layer. On the other hand, the characteristics of EOT and dielectric constant of $La_2O_3/Al_2O_3/Si$ films are ideally. The dielectric constant (10.59) of $La_2O_3/Al_2O_3/Si$ before annealing is higher than the theoretical values of dielectric constant of Al_2O_3 ($\sim$9) film. This caused by a good quality of interface layer and the high permittivity values of La_2O_3 films. The La_2O_3 layer that deposited on the top of $La_2O_3/Al_2O_3/Si$ film reacted to moisture and formed $La(OH)_3$ which possess low dielectric constant. Overall, the formation of complicated interfacial layer has had a bigger influence on the whole property of $Al_2O_3/La_2O_3/Si$ films, the characteristics of films have improved after annealing; on the other hand, the formation of $La(OH)_3$ that exposing to the air long time and during RTA process has had a bigger influence on the whole property of $La_2O_3/Al_2O_3/Si$ film.

4 Conclusions

Preliminary results in the development of ALD-grown $La_2O_3\backslash Al_2O_3\backslash Si$ and $Al_2O_3\backslash La_2O_3\backslash Si$ films serving as MIS capacitance are presented. The influences of RTA on the physical and electrical characteristics of different deposition sequences of $La_2O_3\backslash Al_2O_3\backslash Si$ and $Al_2O_3\backslash La_2O_3\backslash Si$ films are investigated. First of all, the content of C and N impurities is low and surface uniformity is perfect for $La_2O_3\backslash Al_2O_3\backslash Si$ and $Al_2O_3\backslash La_2O_3\backslash Si$ films deposited by ALD. All films are deposited on Si substrate with uniform surface morphology according the AFM analyses. Secondly, the dielectric constant, EOT, electrical properties, and stability of $Al_2O_3\backslash La_2O_3\backslash Si$ films are enhanced during RTA process. Dues to the diffusion of La atoms and the hygroscopicity of La_2O_3 film, the EOT increased and the dielectric constant decreased of $La_2O_3\backslash Al_2O_3\backslash Si$ film after annealing. Moreover, the characteristics of $La_2O_3\backslash Al_2O_3\backslash Si$ films are superior to characteristics of $Al_2O_3\backslash La_2O_3\backslash Si$ before and after annealing according to the values of EOT, dielectric constant and XPS analysis. Overall, the

formation of complicated interfacial layer has had a bigger influence on the whole property of $Al_2O_3/La_2O_3/Si$ films; the formation of $La(OH)_3$ that exposing to the air long time and during RTA process has had a bigger influence on the whole property of $La_2O_3/Al_2O_3/Si$ film. Generally, we think that $La_2O_3\backslash Al_2O_3\backslash Si$ and $Al_2O_3\backslash La_2O_3\backslash Si$ films are most promising candidate high-*k* dielectrics for highly scaled MOS transistors.

Acknowledgments This work is supported supported by the Project of National Natural Science Foundation of China (Grant Nos. 61376099, 11235008, 61434007) and the Specialized Research Fund for the Doctoral Program of High Education (Grant No. 20130203130002).

References

1. H.K. Kim, H.S. Jung, J.H. Jang, J. Park, T.J. Park, S.H. Lee, C.S. Hwang, J. Appl. Phys. **110**, 114107 (2011)
2. L. Lamagna, C. Wiemer, M. Perego, S.N. Volkos, S. Baldovino, D. Tsoutsou, S. Schamm-Chardon, P.E. Coulon, M. Fanciulli, J. Appl. Phys. **108**, 084108 (2010)
3. M. Suzuki, T. Yamaguchi, N. Fukushima, M. Koyama, J. Appl. Phys. **103**, 034118 (2008)
4. B. Lee, T.J. Park, A. Hande, M.J. Kim, R.M. Wallace, J. Kim, X. Liu, J.H. Yi, H. Li, M. Rousseau, D. Shenai, J. Suydam, Microelectron. Eng. **86**, 1658 (2009)
5. J.W. Liu, M.Y. Liao, M. Imura, H. Oosato, E. Watanabe, Y. Koide, Appl. Phys. Lett. **102**, 112910 (2013)
6. S. McDonnell, A. Pirkle, J. Kim, L. Colombo, R.M. Wallace, J. Appl. Phys. **112**, 104110 (2012)
7. X. Qin, L. Cheng, S. McDonnell, A. Azcatl, H. Zhu, J. Kim, R.M. Wallace, J. Mater. Sci. Mater. Electron. **26**, 4638 (2015)
8. J.B. Fan, H.X. Liu, B. Gao, F. Ma, Q.Q. Zhuo, Y. Hao, Chin. Phys. B **21**, 087702 (2012)
9. X. Fan, H. Liu, X. Zhang, Appl. Phys. A **114**, 545 (2013)
10. K.B. Jinesh, J.H. Klootwijk, Y. Lamy, R. Wolters, E. Tois, M. Tuominen, F. Roozeboom, W.F.A. Besling, Appl. Phys. Lett. **93**, 172904 (2008)
11. S. Abermann, O. Bethge, C. Henkel, E. Bertagnolli, Appl. Phys. Lett. **94**, 262904 (2009)
12. M. Nath, A. Roy, Phys. B **482**, 43 (2016)
13. P.K. Sarkar, M. Prajapat, A. Barman, S. Bhattacharjee, A. Roy, J. Mater. Sci. **51**, 4411 (2016)
14. L. Wu, Y. Zhang, H. Lu, Y. Zhang, Jpn. J. Appl. Phys. **54**, 110303 (2015)
15. C.L. Cheng, C.C. Liu, K.-S. Chang-Liao, J. Vac. Sci. Technol. B **31**, 022204 (2013)
16. T. Das, C. Mahata, C.K. Maiti, E. Miranda, G. Sutradhar, P.K. Bose, Appl. Phys. Lett. **98**, 022901 (2011)
17. J.W. Ma, W.J. Lee, M.-H. Cho, K.M. Lee, H.C. Sohn, C.S. Kim, H.J. Cho, Appl. Phys. Lett. **109**, 124106 (2011)
18. H. Gou, S. Chen, S. Ding, Q. Sun, H. Lu, D. Zhang, P. Wang, Thin Solid Films **529**, 380 (2013)
19. W.F. Xiang, Y.Z. Liu, H.B. Lu, L. Yan, M. He, Z.H. Chen, Thin Solid Films **515**, 2722 (2006)
20. M. Suzuki, Materials **5**, 443 (2012)
21. P. Sivasubramani, M.J. Kim, B.E. Gnade, R.M. Wallacea, Appl. Phys. Lett. **86**, 201901 (2005)
22. T.J. Park, P. Sivasubramani, B.E. Coss, H.C. Kim, B. Lee, R.M. Wallace, J. Kim, M. Rousseau, X. Liu, H. Li, J.S. Lehn, D. Hong, D. Shenai, Appl. Phys. Lett. **97**, 092904 (2010)
23. W.J. Lee, J.W. Ma, J.M. Bae, C.Y. Kim, K.S. Jeong, M.-H. Cho, K.B. Chung, H. Kim, H.J. Cho, D.C. Kim, Curr. Appl. Phys. **13**, 633 (2013)
24. Z.-Y. Ye, H.-L. Lu, Y. Geng, Y.-Z. Gu, Z.-Y. Xie, Y. Zhang, Q.-Q. Sun, S.-J. Ding, D.W. Zhang, Nanoscale Res. Lett. **8**, 108 (2013)
25. J.W. Liu, M.Y. Liao, M. Imura, H. Oosato, E. Watanabe, A. Tanaka, H. Iwai, Y. Koide, J. Appl. Phys. **114**, 084108 (2013)
26. W.J. Maeng, W.H. Kim, H. Kim, J. Appl. Phys. **107**, 074109 (2010)
27. H. Jin, Y.J. Cho, S.K. Oh, H.J. Kang, J.C. Park, S. Heo, J.C. Lee, Appl. Phys. Lett. **93**, 052904 (2008)
28. B. Lee, S.R. Novak, D.J. Lichtenwalner, X. Yang, V. Misra, IEEE Trans. Electron. Devices **58**, 3106 (2011)
29. D. Eom, C.S. Hwang, H.J. Kim, M.-H. Cho, K.B. Chungc, Electrochem. Solid State **11**, G33 (2008)
30. C.K. Chiang, C.H. Wu, C.C. Liu, J.F. Lin, C.L. Yang, J.Y. Wu, S.J. Wang, J. Electrochem. Soc. **158**, H447 (2011)
31. L. Calmels, P.E. Coulon, S. Schamm-Chardon, Appl. Phys. Lett. **98**, 243116 (2011)